Supporting Information

Dibenzothiophene sulfone-based n-type emissive organic semiconductor

Xianneng Chen,[†ab] Qingbin Li,[†*b] Yumin Liu,[b] Shaoqing Guan,[bc] Pu Wang,[bc] Ziyi Xie,[bc] Xiangyu Tan,[b] Dan Liu,[b] Molin Shen,[bc] Can Gao,[b] Shiming Zhang,*[ad] Huanli Dong *[bc]

[a] Key Laboratory of Flexible Electronics (KLOFE) & Institute of Advanced Materials (IAM), Jiangsu National Synergetic Innovation, Center for Advanced Materials (SICAM), Nanjing Tech University, Nanjing, Jiangsu 211816, China.

[b] Beijing National Laboratory for Molecular Sciences, Key Laboratory of Organic Solids, Institute of Chemistry, Chinese Academy of Sciences Beijing 100190 China.

[c] University of Chinese Academy of Sciences, Beijing 100190, China.

[d] City University of Hong Kong (Dongguan), 8 Gaoxiong Road, Dongguan, Guangdong 523808, China.

E-mail: dhl522@iccas.ac.cn; iamsmzhang@njtech.edu.cn; benaini@iccas.ac.cn.

Table of Contents

1. Materials, Preparation and General Characterization Methods.

All chemical reagents and solvents used in this work were purchased from J&K Chemical Co., Energy Chemical Co., Innochem Co., and Sigma-Aldrich Co., and were used without further purification. Column chromatography silica gel was obtained from Qingdao Haiyang Chemical Co., Ltd. ^{1}H NMR spectra and ^{13}C NMR spectra were recorded using a Bruker AVANCE 400II MHz NMR spectrometer. High-resolution MALDI-FTICR-MS was measured by the analytical testing center of the Institute of Chemistry, Chinese Academy of Sciences.

UV/Vis absorption spectra and photoluminescence spectra were collected using a Shimadzu UV-3600 spectrophotometer and Jasco FP-660 spectrofluorometer, respectively. Fluorescence quantum yields were determined using an FLS980 steady-state and transient fluorescence spectrometer. Ultraviolet photoelectron spectroscopy (UPS) was performed on the KRATOS Axis Ultra DLD multifunctional photoelectron spectroscopy platform at the Institute of Chemistry, Chinese Academy of Sciences. The sample for UPS measurement was prepared by depositing a 15nm thin film of DPIDBSO on clean, bare silicon substrates (size:1 cm x 1 cm) The highest occupied molecular orbital (HOMO) and lowest unoccupied molecular orbital (LUMO) were calculated using density functional theory (DFT) at B3LYP/6-31g (d, p) level.[1]

OFET and OLET substrate preparation: 300 nm Si/SiO_2 wafers were first laser-cut into 1 cm×1 cm and 1.5 cm×1.5 cm pieces using a laser marking system. The cut substrates were then immersed in piranha solution (3:7 v/v H_2O_2/H_2SO_4) and heated to boiling for 15 minutes. After cooling to room temperature, the substrates were thoroughly rinsed with ultrapure water, followed by sequential ultrasonic cleaning in acetone and isopropanol. The cleaned substrates were dried under a nitrogen stream for subsequent use. The dried substrates were treated with oxygen plasma and then spin-coated with PMMA solution for device fabrication. The dried substrates were treated with oxygen plasma and then spin-coated (4000 rpm for 60 s) with PMMA solution and annealed at 90 ℃ for device fabrication. The

molecular weight of PMMA is about 350,000 and the concentration of PMMA solution is 6 mg ml^{-1} in chlorobenzene. The thick of PMMA layer is about 20 nm.

The electrodes were constructed by gold strip method. The gold electrodes were formed by evaporating gold on substrate with a shadow mask (thickness: ~200 nm). The silver electrodes were also prepared by first evaporating a 20 nm layer of silver, followed by the deposition of a 180 nm layer of gold onto the substrate using a shadow mask.

All electrical characterizations were conducted in Nitrogen atmosphere glove box using an FS-380 semiconductor test system. The charge carrier mobility was calculated from the saturation regime of transfer characteristics using equation: $I_{ds} = C_i\mu(W/2L)\ (V_G - V_T)$.[2]

The electroluminescence spectrum can be collected using a spectrometer from Ocean Optics, and the acquisition of EQE is completed by collecting the photoelectric current signals through a photomultiplier tube (PMT); EQE can be obtained from the ratio of the number of collected photons ($n_υ$) to the number of injected carriers (n_e):

$$EQE = \frac{n_\upsilon}{n_e}\#...(2.1)$$

The detailed calculation process is as follows: The number of collected photons ($n_υ$) can be calculated from the photocurrent obtained by the PMT, but needs to be calibrated. The photocurrent (I_{PMT}) measured by the PMT has the following relationship when a standard light source is used for testing:

$$I_{PMT} = \int P_C(\lambda)\eta(\lambda)d\lambda = \int P_C(\lambda)B\tilde{\eta}(\lambda)d\lambda\#...(2.2)$$

Here, $P_c(\lambda)$ is the known optical power spectrum of the standard light source, while $\eta(\lambda)$ and $\tilde{\eta}(\lambda)$ denote the spectral response curve and the normalized spectral response curve of the PMT detector, respectively. Then the parameter B can be calculated using equation (2.2). The optical power spectrum of the sample, $P_S\ (\lambda)$

can be normalized as $P_s(\lambda) = AP_S(\lambda)$, where $P_S(\lambda)$ is directly measured by the spectrometer. Similarly, the photocurrent obtained from the sample follows the relationship:

$$I_{PMT} = \int A\tilde{P}_S(\lambda)B\tilde{\eta}_s(\lambda)d\lambda \#...(2.3)$$

The value of A can be determined using equation (2.3), enabling the calculation of the sample's optical power spectrum $P_s(\lambda)$. The number of collected photons can then be obtained through the following expression:

$$n_\upsilon = \int \frac{P_S(\lambda)\lambda d\lambda}{hc} \#...(2.4)$$

Here, h is Planck's constant, c is the speed of light, and the integration range corresponds to the electroluminescence spectrum of the sample. The number of injected carriers (n_e) can be calculated from the source-drain current measured in the OLET device as $n_e = I_{ds}/e$. Substituting this and equation (2.4) into equation (2.1) yields the external quantum efficiency (EQE):

$$EQE = \frac{\int \frac{eP(\lambda)\lambda}{hc} d\lambda}{I_{ds}} \#...(2.5)$$

2. Synthesis

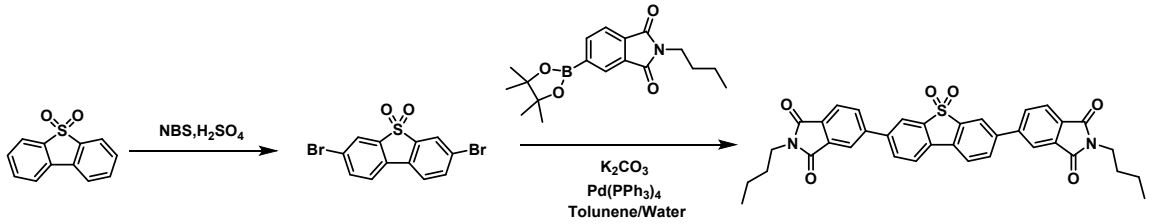

Scheme S1. Synthesis of DPIDBSO.

3-bromodibenzo[b,d]thiophene 5,5-dioxide：Dissolve 5 g of dibenzothiophene sulfone in a round-bottom flask containing 100 mL of concentrated sulfuric acid at 0 °C. 8.2 g of *N*-bromosuccinimide (NBS) was added into flask in batches, and then stir the mixture at room temperature for 16 hours. After reaction, the reaction mixture was poured into ice water, followed by extraction with chloroform. Dry the solution over anhydrous magnesium sulfate and remove the solvent under reduced pressure. Finally, the crude product was purified through column chromatography

using dichloromethane/petroleum ether mixture (1:1), yielding 7.8 g product as a white solid (yield: 87%). This step refers to the literature.[3]

5,5'-(5,5-dioxidodibenzo[b,d]thiophene-3,7-diyl)bis(2-butylisoindoline-1,3-dione) (DPIDBSO)：In a 50 mL round-bottom flask under an argon atmosphere, 2-butyl-5-(4,4,5,5-tetramethyl-1,3,2-dioxaborolan-2-yl) isoindoline-1,3-dione (500 mg, 2.06 mmol), 3,7-dibromodibenzo[b,d]thiophene 5,5-dioxide (880 mg, 2 equivalents), tetrakis(triphenylphosphine)palladium (247.15 mg, 0.2 equivalents), and potassium carbonate (1.108 g, 6 equivalents) were added. Subsequently, inject 16 mL of degassed toluene and 4 mL of water into the mixture. Then stir the mixture at 90 °C for 25 hours. After the reaction, the mixture was washed with water, extract with chloroform, and dry over anhydrous magnesium sulfate before removing the solvent under reduced pressure. The product was purified using column chromatography with chloroform, yielding 360 mg white solid (Yield: 43%). ^{1}H NMR (400 MHz, $CDCl_3$): δ 8.11 (s, 4H), 7.94-8.00 (m, 8H), 3.74 (t, 4H), 1.66-1.74 (m, 4H), 1.37-1.43 (m, 4H), 0.97 (t, 6H). ^{13}C NMR (101 MHz, $CDCl_3$) δ167.92, 144.55, 142.00, 139.24, 133.42, 132.99, 132.45, 131.86, 131.08, 124.08, 122.69, 121.70, 121.14, 38.10, 30.65, 20.13, 13.69. HRMS (MALDI-FT-ICR): $[M+H]^+$ calcd. for $C_{36}H_{30}N_2O_6S$, 619.189734; found 619.190001. Elemental analysis: Anal. calculated: C: 69.89%, H: 4.89%, S: 5.18% N: 4.53%. Experimental: C: 69.82%, H: 4.78%, S: 5.38%, N: 4.51%.

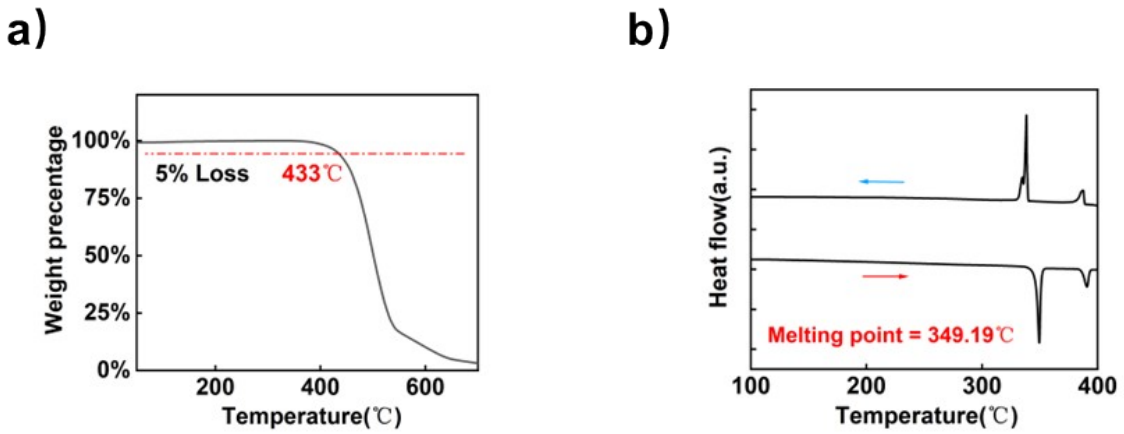

Figure S1. (a) Thermogravimetric analysis and (b) Differential scanning calorimetry of DPIDBSO.

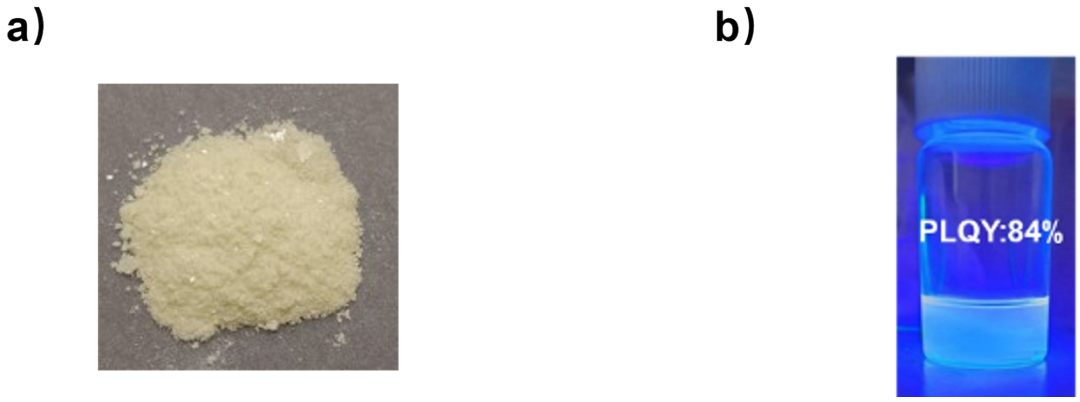

Figure S2. a) Image of DPIDBSO powder obtained through sublimation purification. b) Photoluminescence image of DPIDBSO in chloroform solution under UV light (365 nm).

Table S1 Summary of optical properties for DPIDBSO.

DPIDBSO	PLQY（%）	τ（ns）	k_r （s^{-1}）
Solution	84	1.35	6.4×10^8
Powder	30	2.47	1.2×10^8

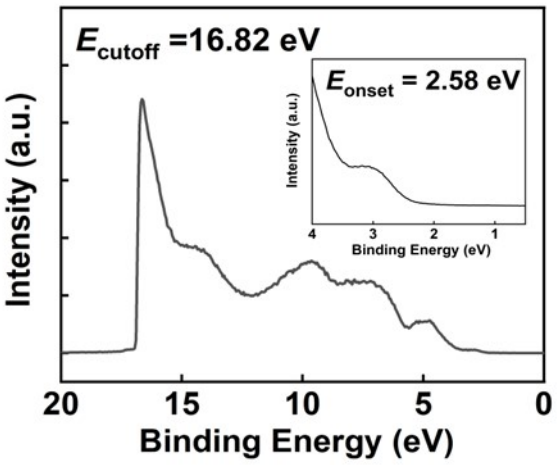

Figure S3. UPS energy distribution curve of DPIDBSO (E_{HOMO} = -21.2 + (E_{cutoff} - E_{onset})).

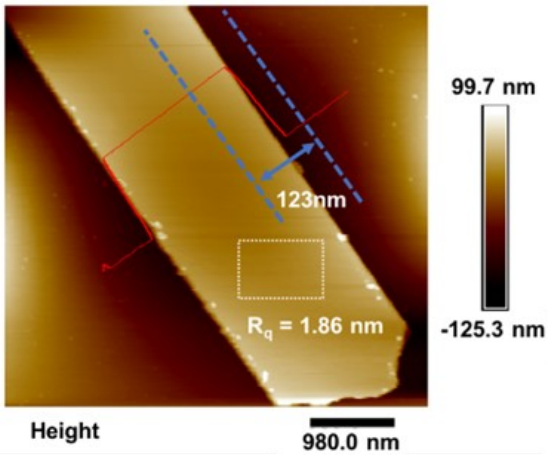

Figure S4. The AFM image of DPIDBSO crystals (Rq is the root mean square roughness; The thickness of crystal is about 120 nm).

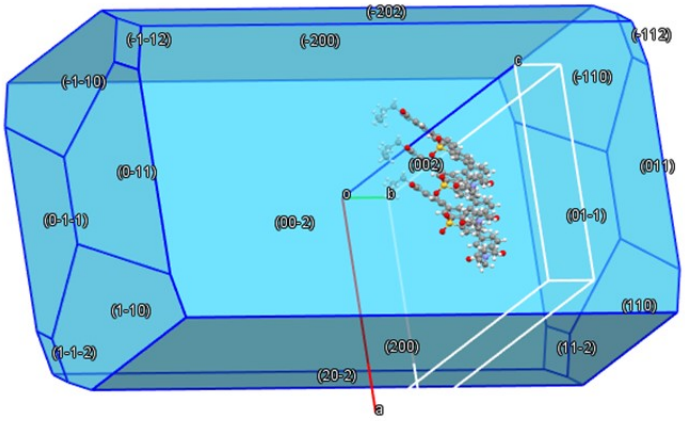

Figure S5. Crystal morphology of DPIDBSO simulated by the Bravais–Friedel–Donnay-Harker method.

Table S2 Summary of transfer integrals of DPIDBSO based on crystal structure.

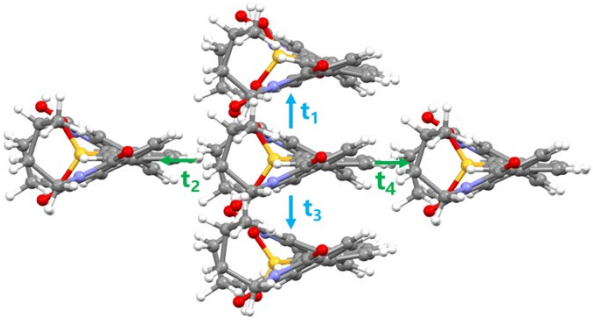

Electronic coupling	LUMO-LUMO（meV）
t_1	-40.226
t_2	-10.679
t_3	-40.229
t_4	-10.681

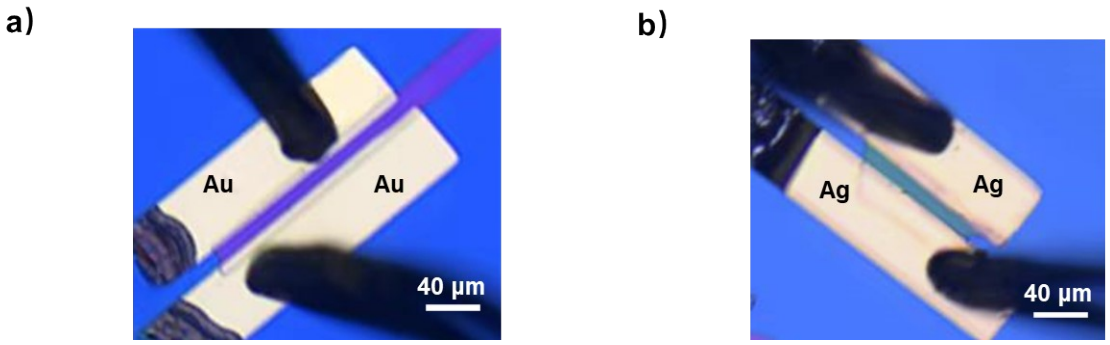

Figure S6. Examples for DPIDBSO-based devices with (a) Au electrodes or (b) Ag electrodes along *a*-axis.

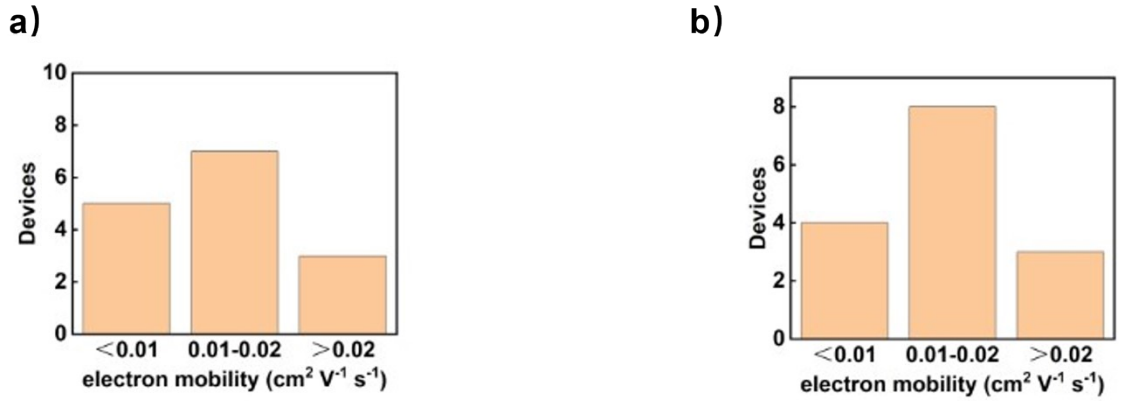

Figure S7. Electron mobility statistics chart for DPIDBSO devices with a) Au electrodes and b) Ag electrodes along *a*-axis.

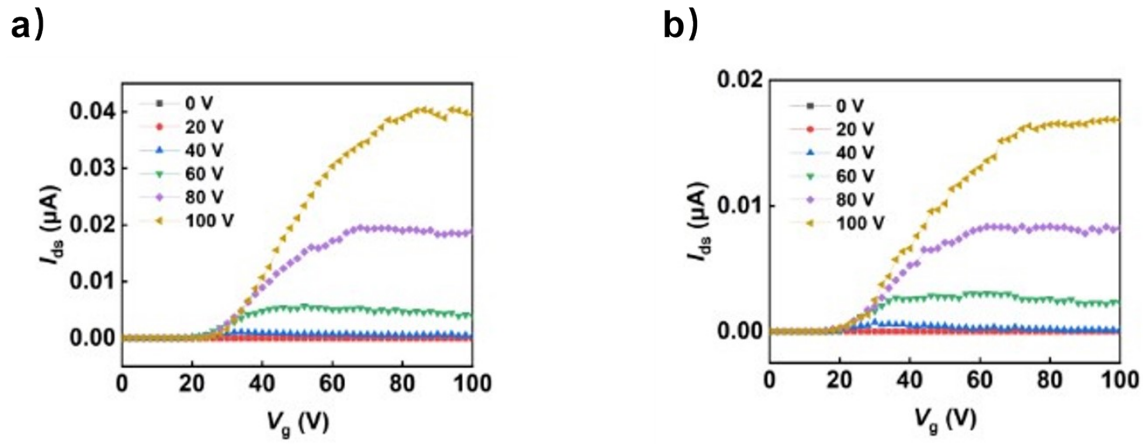

Figure S8. Typical output curves of DPIDBSO devices with a) Au electrodes and b) Ag electrodes along *a*-axis.

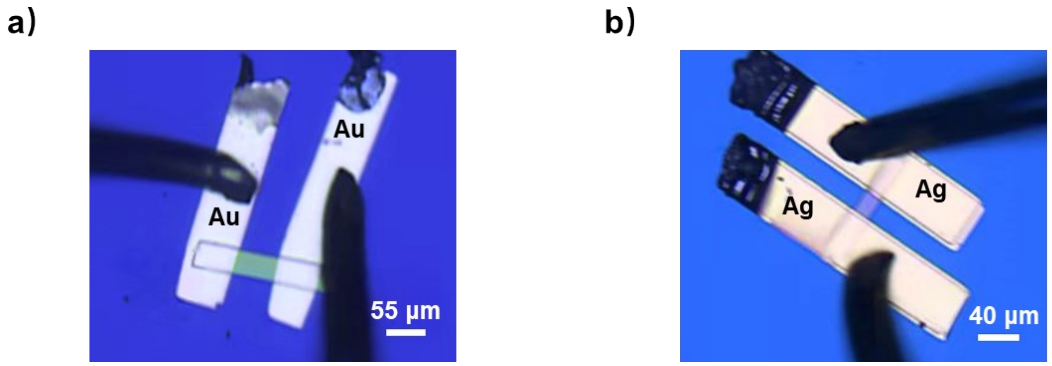

Figure S9. Examples of DPIDBSO devices with a) Au electrodes and b) Ag electrodes along *b*-axis.

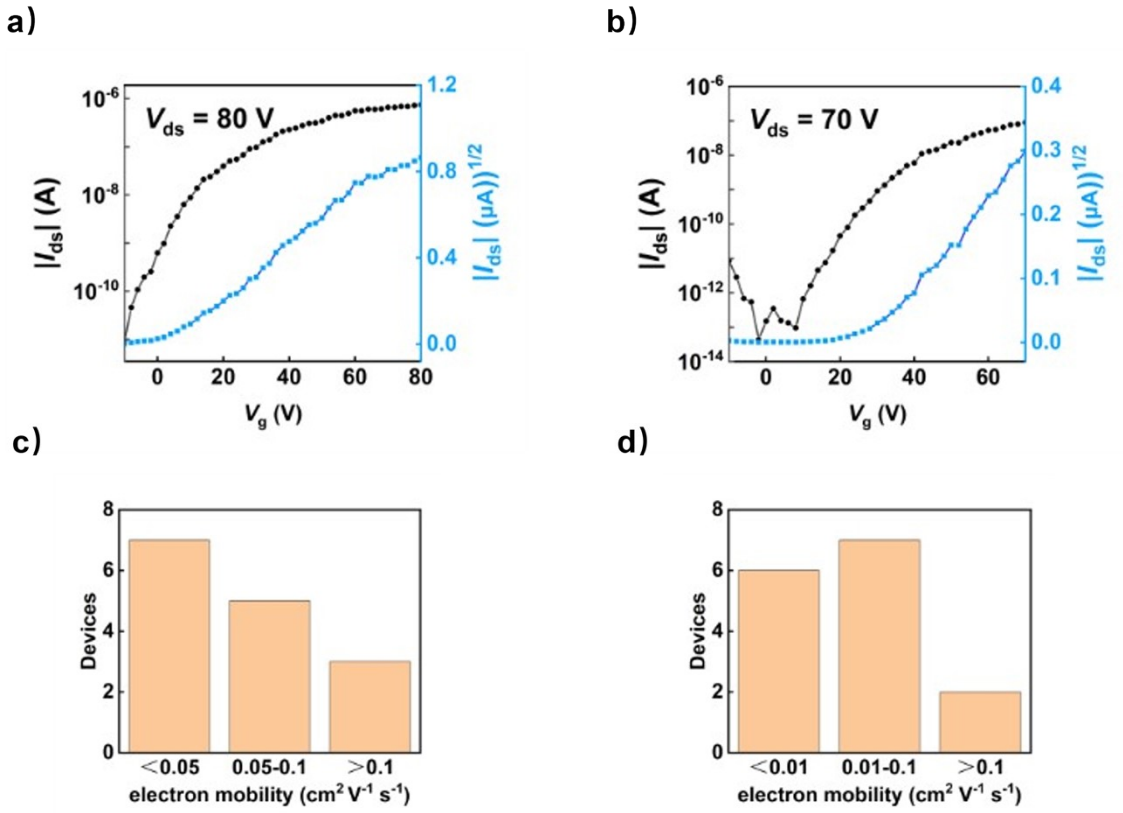

Figure S10. Typical transfer curves for DPIDBSO devices with a) Au electrodes and b) Ag electrodes along *b*-axis. Electron mobility statistics chart for DPIDBSO devices with c) Au electrodes and d) Ag electrodes along *b*-axis.

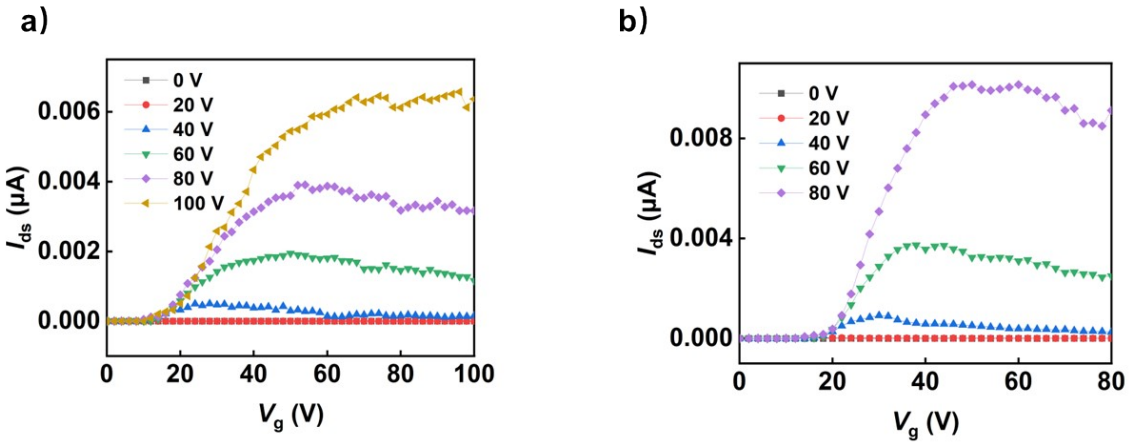

Figure S11 Typical output curves of DPIDBSO devices with a) Au electrodes and b) Ag electrodes along *b*-axis.

Table S3 Summary of electron mobility of DPIDBSO.

Electrode	Au		Ag	
	μ_{max} ($cm^2 V^{-1} s^{-1}$)	$\mu_{ave.}$ ($cm^2 V^{-1} s^{-1}$)	μ_{max} ($cm^2 V^{-1} s^{-1}$)	$\mu_{ave.}$ ($cm^2 V^{-1} s^{-1}$)
***a*-axis**	0.02	0.01	0.07	0.01
***b*-axis**	0.13	0.05	0.17	0.02

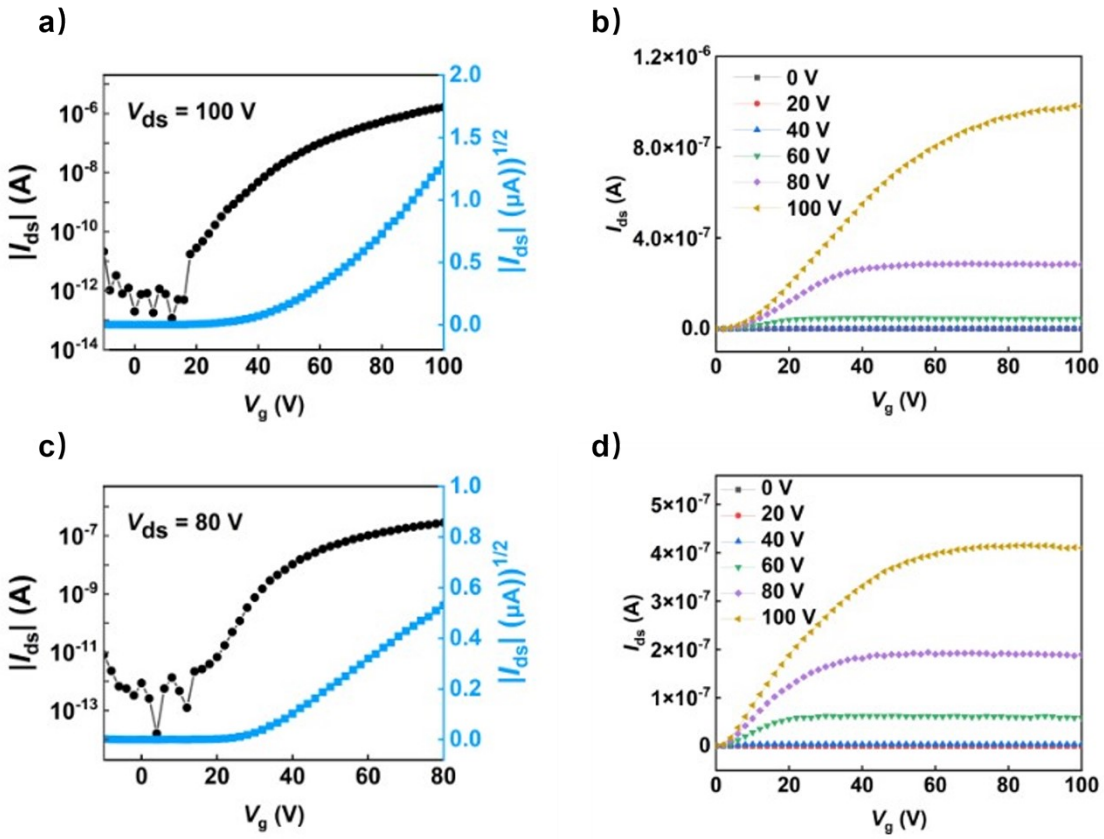

Figure S12 a) Typical transfer curves and b) typical output curves of devices with evaporated silver electrodes along *a*-axis. c) Typical transfer curves and d) typical output curves of devices with evaporated silver electrodes along *b*-axis.

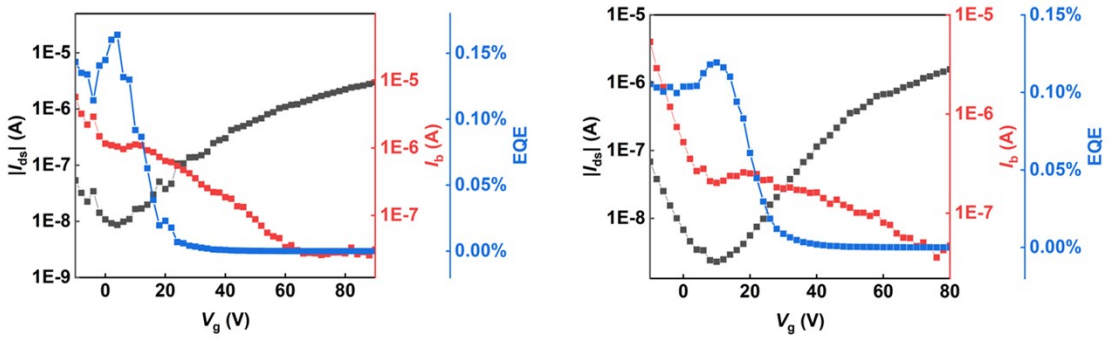

Figure S13 Some examples for typical transfer curves, normalized PMT photocurrent (I_b) and EQE of devices with Ag electrodes.

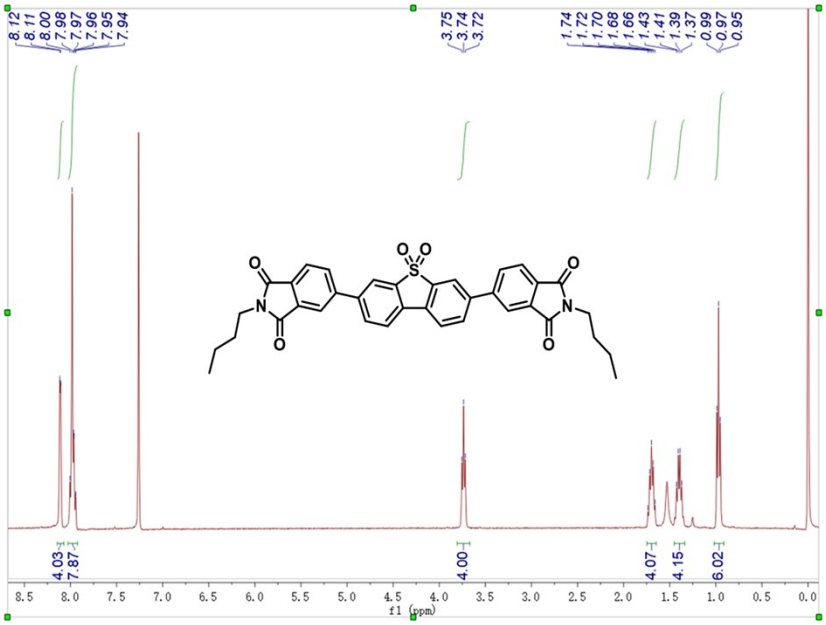

Figure S14. ^{1}H NMR spectrum of DPIDBSO in $CDCl_3$.

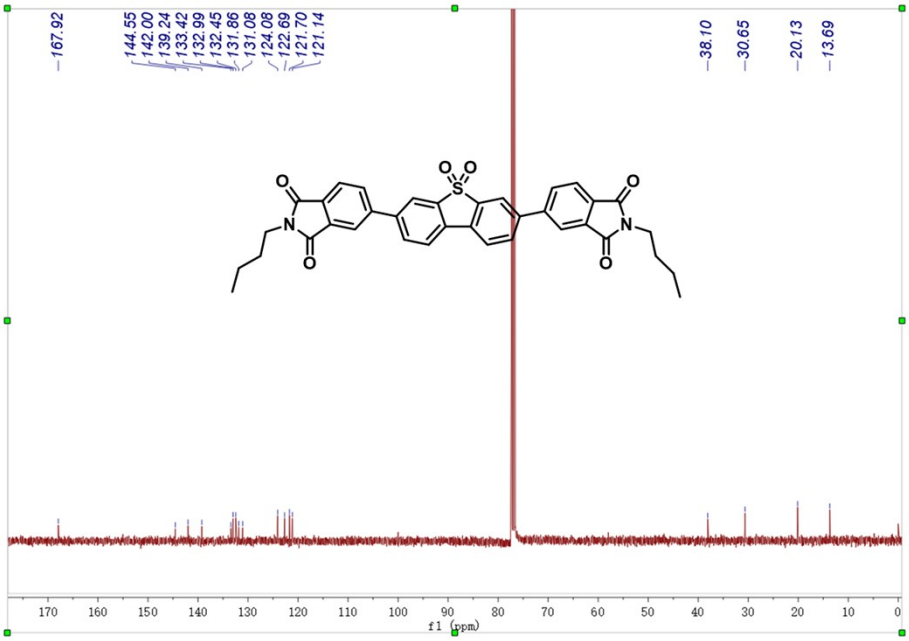

Figure S15. ^{13}C NMR spectrum of DPIDBSO in $CDCl_3$

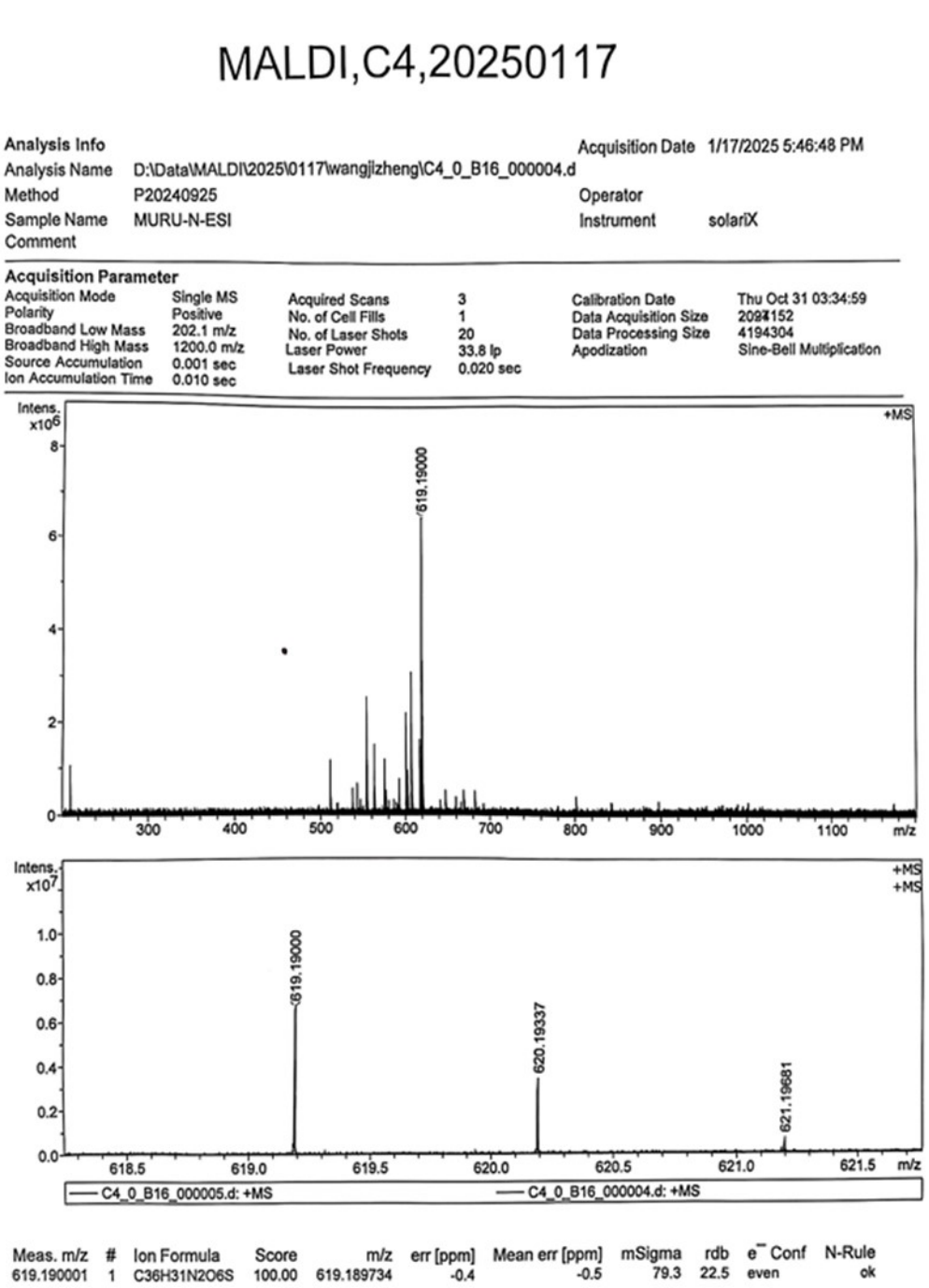

Figure S16 High-resolution mass spectrometry of DPIDBSO.

Table S4 Crystal data and structure refinement for DPIDBSO.

Parameters	DPIDBSO
Empirical formula	$C_{36}H_{30}N_2O_6S$
Formula weight	618.68
Temperature/K	170.15
Crystal system	monoclinic
Space group	I2/a
a/Å	28.8789(17)
b/Å	7.3439(4)
c/Å	41.767(2)
α/°	90
β/°	100.278(5)
γ/°	90
Volume/Å^3	8716.0(8)
Z	12
ρ_{calc}g/cm^3	1.414
μ/mm^{-1}	1.431
F (000)	3888.0
Crystal size/mm^3	0.2 × 0.15 × 0.1
Radiation	CuKα (λ = 1.54184)
2θ range for data collection/°	6.22 to 155.98
Index ranges	-36 ≤ h ≤ 34, -9 ≤ k ≤ 9, -50 ≤ l ≤ 52
Reflections collected	44809
Independent reflections	8874 [R_{int} = 0.1250, R_{sigma} = 0.0789]
Data/restraints/parameters	8874/0/612
Goodness-of-fit on F^2	1.044
Final R indexes [I>=2σ (I)]	R_1 = 0.0973, wR_2 = 0.2590
Final R indexes [all data]	R_1 = 0.1564, wR_2 = 0.3121
Largest diff. peak/hole / e Å^{-3}	0.82/-0.57

References

1. a) R. Dennington, T. A. Keith, J. M. Millam, GaussView, Version 6.1. 2019; b) M. J. Frisch, G. W. Trucks, H. B. Schlegel, G. E. Scuseria, M. A. Robb, J. R. Cheeseman, G. Scalmani, V. Barone, G. A. Petersson, H. Nakatsuji, X. Li, M. Caricato, A. Marenich, J. Bloino, B. G. Janesko, R. Gomperts, B. Mennucci, H. P. Hratchian, J. V. Ortiz, A. F. Izmaylov, J. L. Sonnenberg, D. Williams-Young, F. Ding, F. Lipparini, F. Egidi, J. Goings, B. Peng, A. Petrone, T. Henderson, D. Ranasinghe, V. G. Zakrzewski, J. Gao, N. Rega, G. Zheng, W. Liang, M. Hada, M. Ehara, K. Toyota, R. Fukuda, J. Hasegawa, M. Ishida, T. Nakajima, Y. Honda, O. Kitao, H. Nakai, T. Vreven, K. Throssell, J. A. Montgomery, Jr., J. E. Peralta, F. Ogliaro, M. Bearpark, J. J. Heyd, E. Brothers, K. N. Kudin, V. N. Staroverov, T. Keith, R. Kobayashi, J. Normand, K. Raghavachari, A. Rendell, J. C. Burant, S. S. Iyengar, J. Tomasi, M. Cossi, J. M. Millam, M. Klene, C. Adamo, R. Cammi, J. W. Ochterski, R. L. Martin, K. Morokuma, O. Farkas, J. B. Foresman, D. J. Gaussian 16 Rev. C.01, Wallingford, CT, 2016.

2. X. Tan, Q. Li, Z. Qin, D. Liu, Y. Liu, P. Wang, Z. Xie, Z. Miao, Y. Lei, Y. Zhang, P. Wang, X. Chen, Z. Liu, C. Gao, W. Hu, H. L. Zhang and H. Dong, *Mater Horiz*, 2025, **12**, 1589.

3. Q. Li, Y. Zhang, J. Lin, Y. Zou, P. Wang, Z. Qin, Y. Wang, Y. Li, Y. Zhang, C. Gao, Y. Zang, W. Hu and H. Dong, *Angew Chem Int Ed.*, 2023, **62**, e202308146.